# Directional coupler wavelength filters based on waveguides exhibiting electromagnetically induced transparency

Marcelo Davanço, Petter Holmström, Daniel J. Blumenthal and Lars Thylén

*Abstract*— **We describe the principle and analyze the operation of an integrated optics directional coupler filter based on coupling between a regular waveguide and one that exhibits electromagnetically induced transparency. Bandwidth length products on the order of 2 $pm \times mm$ are obtainable, as an example, using this approach.**

*Keywords*— **Electromagnetically Induced Transparency, Directional Couplers, Nonlinear Optics**

## I. INTRODUCTION

Optical waveguide filters are important devices in wavelength division multiplexing (WDM) systems. For dense WDM, rather narrow filter bandwidths are required for the proper treatment of channels in a standard frequency grid (e.g. 10-50 GHz bandwidth in a 100 GHz grid). Moreover, the filter should preferably be of a non-reflective type and, in fact, have low return losses.

Arrayed waveguide gratings [1] are one class of filters that exhibit the desired performance in this respect, but for functions such as add-drop-multiplexers, simpler and, above all, significantly more compact devices are essential. Directional coupler filters based on differential dispersion have been researched for a number of years (see e.g. [2]) and are lately used in widely tunable lasers [3]. In these filters, the bandwidth is inversely proportional to the length of the coupler as well as to the differential dispersion at the wavelength of phase matching (equal effective indices $N_{eff}$). However, the bandwidths have been limited to several nanometers over 1 $mm$ length due to the difficulty of achieving large differential dispersion in conventional waveguides.

Couplers where one of the waveguides is made of a material which exhibits electromagnetically induced transparency (EIT) [4] offer, when suitably pumped, novel possibilities to engineer dispersion. Huge dispersions can in fact be obtained, and thus very narrow filter bandwidths.

In this paper we first review the principle of operation of directional coupler filters, then briefly discuss the relevant features of EIT, notably the susceptibilities, which are used as a basis for bandwidth calculations. We then analyze filter design using EIT and finally the prospects for the realization of these devices are discussed.

M. Davanço and D.J. Blumenthal are with the Optical Communications and Photonic Networks Group, Electrical and Computer Engineering Dept., University of California Santa Barbara, Santa Barbara CA 93106.

P. Holmström and L. Thylén are with the Laboratory of Photonics and Microwave Engineering, Dept. of Microelectronics and Information Technology, Royal Institute of Technology (KTH), SE-164 40 Kista-Stockholm, Sweden.

Contact email: mdavanco@ece.ucsb.edu

## II. Directional coupler filter bandwidth

### A. Filter bandwidth

We consider a coupler consisting of two slab waveguides, 1 (input) and 2 (output), respectively with phase indices $n_{1p}$, $n_{2p}$, separated by a distance $l$ and surrounded by a substrate material with phase index $n_{sp}$, such as shown in Figure 1. Taken separately, guides 1 and 2 are designed to have only one guided mode each, with effective propagation constants $\beta_1$ and $\beta_2$, respectively, corresponding to mode effective indexes $N_{1p}$ and $N_{2p}$. Considering the

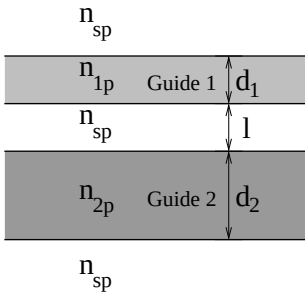


Fig. 1. Waveguide coupler filter strucutre

guides to be sufficiently distant from each other so that only a weak coupling between them exists, the following expression is obtained from coupled-mode theory [5], describing the squared amplitude of a mode inside waveguide 2:

$$|a_2(z)|^2 = \left(\frac{\kappa_{21}}{2s}\sin sz\right)^2 \tag{1}$$

Here,

$$s = \sqrt{\left(\frac{\beta_1 - \beta_2}{2}\right)^2 + \kappa_{12}\kappa_{21}}, \tag{2}$$

$\kappa_{12}$ and $\kappa_{21}$ are the coupling coefficients between the guides and $z$ is the spatial displacement along the coupler. Maximum power transfer from input to output will happen at a frequency $\omega_0$ for which the two propagation constants are equal. This is chosen to be the operation frequency of the device. Also, the coupler length must be

$$L = \frac{\pi}{2\sqrt{\kappa_{12}\kappa_{21}}}. \tag{3}$$

At $z = L$, for $\omega$ near $\omega_0$, the change in the argument of (1) with wavelength $\lambda$ is given by

$$\Delta(sL) \approx \frac{L}{2}\frac{d}{d\lambda}(\beta_1 - \beta_2)\,\Delta\lambda = \frac{L}{2}(N_{2g} - N_{1g})\frac{2\pi}{\lambda_0^2}\Delta\lambda, \quad (4)$$

assuming that the coupling coefficients change very little with $\lambda$; so a bandwidth $\Delta\lambda$ of the filter can be defined as

$$\Delta\lambda = \lambda - \lambda_0 = \frac{\lambda_0^2}{L(N_{2g} - N_{1g})}, \quad (5)$$

where

$$N_{1,2g} = N_{1,2p} - \lambda\frac{dN_{1,2p}}{d\lambda} \quad (6)$$

are the group indexes of modes in waveguides 1 and 2, taken at the center frequency. It is apparent that the bandwidth could be made arbitrarily small by choosing guides with propagation constants that change with frequency (or wavelength) at sufficiently different rates around the operation frequency. The total dispersion in the waveguides has contributions both from the material and waveguiding mechanism; as will be shown below, the material dispersion of an EIT medium can be tuned to very high values through optical pumping.

Slab waveguides were chosen for simplicity, since analytical expressions for many of the relevant quantities are easily derived. Also, only the TE case was examined, but similar performance should be expected for TM waves. The following expression for group index, valid for the TE case, was used in the calculations [6]:

$$N_{ig} = \frac{\Gamma_i n_{ig} n_{ip} + (1 - \Gamma_i) n_{sg} n_{sp}}{N_{ip}}; i = 1, 2 \quad (7)$$

In this equation, $\Gamma_i$ is the confinement factor of the mode and $n_{ig}$ is the group index due to material dispersion in guide $i$. Analytical expressions for such group indexes can be found in the literature for some materials of interest. In particular, those of $In_{1-x}Ga_xAs_yP_{1-y}$ compounds are described in [7].

### *B. Filter Design*

One possible coupler filter design is described next, considering $In_{1-x}Ga_xAs_yP_{1-y}$ material lattice-matched to InP, for operation at $\lambda = 1.55\ \mu m$.

The normalized frequencies $V_1$ and $V_2$ of guides 1 and 2 are chosen arbitrarily; such numbers in fact reflect the confinement of the guides' individual modes and will ultimately define the necessary separation between them, as well as the coupling length. By choosing the phase index of guide 2, one obtains the effective index of its fundamental mode. The phase-matching condition at center frequency requires $N_{1p} = N_{2p}$, thence one obtains the phase index of guide 1. A specific phase index can be obtained by changing the composition of the quaternary material [7]. The thickness of both guides, $d_1$ and $d_2$ are obtained next from the respective $V$-numbers. Following this step, the distance $l$ between guides is found by inspection for arbitrary coupler length $L$: for each $d$ within the tested range, the corresponding coupling coefficients are obtained, and, from (3), the coupler lengths are calculated. Finally, the bandwidth defined in (5) is calculated using the obtained $L$ and $N_{1,2g}$ from (7). Parameters of a design example are displayed below:

Chosen parameters:
$L = 1\ mm$, $V_1 = 2.0$, $V_2 = 3.0$, $n_{2p} = 3.44$ $n_{sp} = 3.166$,
Calculated values:
$n_{2g} = 3.72$, $n_{sg} = 3.20$, $N_{1,2p} = 3.34$, $n_{1p} = 3.54$,
$d_1 = 0.312\ \mu m$, $d_2 = 0.55\ \mu m$, $l = 1.66\ \mu m$

The filter bandwidth for this design is $B = 11.503\ nm$.

## III. Electromagnetically induced transparency

Electromagnetically induced transparency can be achieved in materials with three-level electronic systems such as shown in figure 2. As predicted in the literature [4], [8], such materials can be made transparent for optical signals at the frequency of the $a$-$b$ transition (signal field) through appropriate optical pumping at the $a$-$c$ transition frequency (control field). Transparency is a result of a coherent superposition of the eigenstates $|b\rangle$ and $|c\rangle$ in time such that the system is trapped in a time-invariant state - the so-called "dark state". This is possible if the degree of coherence between $|b\rangle$ and $|c\rangle$ in time is sufficiently high. Effectively, no $a$-$b$ transitions occur in this case, in spite of the presence the signal field; the latter will, therefore experience no absorption. The same is valid for the control field.

It is possible to adiabatically drive an initial population of electrons at state $|b\rangle$ into a dark state by, for instance, raising the signal field power while having the control field set at an appropriate power level [4], [8], [9], [10]. In this article, we are primarily interested in looking at the static characteristics of EIT media, and consider the modification of the material losses and dispersion after the establishment of a steady-state.

In figure 2 the Rabi frequencies $\Omega_{ab}$ and $\Omega_{ac}$ relate to the signal and control fields respectively. Field amplitude $\mathcal{E}$ and Rabi frequency $\Omega$ are related as $\Omega = \frac{\mathcal{P}\mathcal{E}}{\hbar}$, with $\mathcal{P}$ an electrical dipole matrix element relating two states (e.g. $\mathcal{P} = e\langle a|r|c\rangle$ for states $a, c$). In order to estimate the optical power densities involved, we relate $\Omega$ to the free-space power density

$$S = \frac{|\mathcal{E}|^2}{Z_0} = \left|\frac{\Omega\hbar}{\mathcal{P}}\right|^2 \frac{1}{Z_0}, \quad (8)$$

with $Z_0 = 377\Omega$ the vacuum impedance.

Applying density matrix formalism to the 3-level system in figure 2, the following expressions are obtained for the real and imaginary parts of the complex susceptibility [4]:

$$\chi' = \frac{N_a|\mathcal{P}_{ab}|^2\Delta}{\epsilon_0\hbar} \times \frac{\gamma_3(\gamma_1 + \gamma_3) + (\Delta^2 - \gamma_1\gamma_3 - \Omega_{ac}^2/4)}{(\Delta^2 - \gamma_1\gamma_3 - \Omega_{ac}^2/4)^2 + \Delta^2(\gamma_1 + \gamma_3)^2} \quad (9)$$

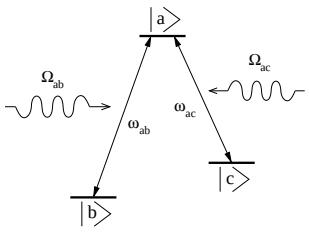


Fig. 2. Three-level system.

$$\chi'' = \frac{N_a|\mathcal{P}_{ab}|^2}{\epsilon_0\hbar}\frac{\Delta^2(\gamma_1+\gamma_3)-\gamma_3(\Delta^2-\gamma_1\gamma_3-\Omega_{ac}^2/4)}{(\Delta^2-\gamma_1\gamma_3-\Omega_{ac}^2/4)^2+\Delta^2(\gamma_1+\gamma_3)^2} \tag{10}$$

where $\Delta = \omega_{ab}-\omega$ is the frequency detuning between signal field and the $a$-$b$ transition frequency, $N_a$ the atom number density, $\mathcal{P}_{ab}$ is the dipole matrix element. The Rabi frequency $\Omega_{ac}$ is related to the control field amplitude. $\gamma_1$ is the decay constant for non-diagonal density operator element $\rho_{ab}$ (ground state-excited state for the signal transition), while $\gamma_3$ is the decay constant for element $\rho_{bc}$, or, ultimately, the dark state.

Real and imaginary parts of the complex index seen by the signal field are shown in figure 3 as functions of frequency, for different values of the control field Rabi frequency $\Omega_{ac}$. Dashed lines show the situation for no applied control field. In this case, the material behaves as a regular 2-state system, showing an absorption peak at the resonance frequency and a rapid change of refractive index with frequency. At the center frequency, electrons in the material are efficiently transferred between states $a$ and $b$, leading to high losses. With an applied control field, after transparency has been established, no transitions occur between these eigenstates, the signal field is not attenuated. As the control power increases, the low-loss frequency range becomes larger and the slope of the propagation constant decreases. The decay rates used in the plots above were $\gamma_1 = 1$ THz, $\gamma_3 = 100$ MHz. We considered also a carrier concentration $N_a = 1\times10^{23}\ m^{-3}$ and transition-matrix element $\mathcal{P}_{ab} = 1\ nm\cdot e$, values typically found in semiconductors.

By inspecting (9) and (10) it is possible to analyze trends imposed by some of the parameters on the material's losses and dispersion for small $\chi$. The material loss in this case relates to the susceptibility as

$$\alpha \approx \frac{k_0\chi''}{n_0}, \tag{11}$$

while the (real) refractive index relates to $\chi'$ as

$$n \approx n_0 + \frac{\chi'}{2n_0}, \tag{12}$$

where the background index $n_0$ corresponds to the polarization from bound charges in the dielectric material. Losses at zero frequency deviation will then vary with

$$\chi''(\omega_{ab}) \propto \frac{N_a|\mathcal{P}_{ab}|^2}{\gamma_1}\frac{1}{1+\frac{\Omega_{ac}^2}{4\gamma_1\gamma_3}}. \tag{13}$$

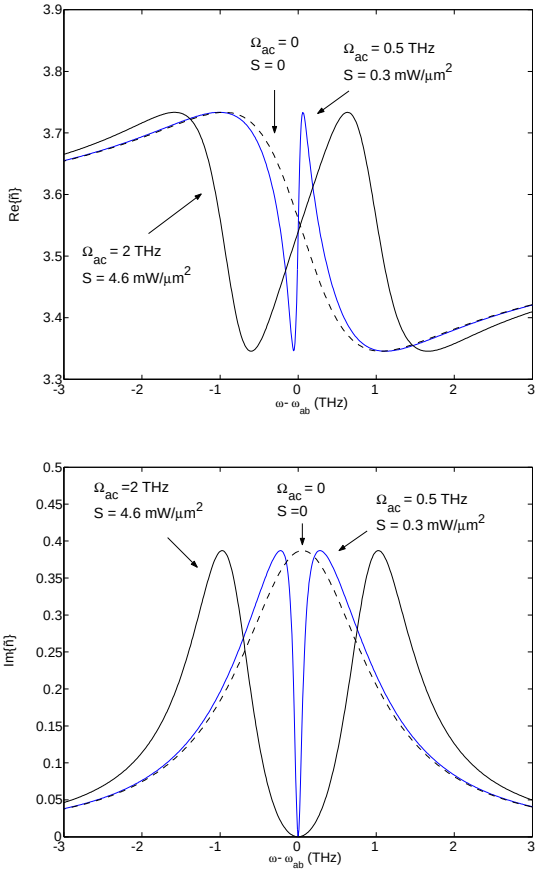


Fig. 3. Real and imaginary parts of the complex refractive index of EIT material at different values. of $\Omega_{ac}$. The corresponding values of power density S are also shown. The horizontal axis represents the displacement from the center frequency. The dashed line indicates the case of no applied control signal.

It is clear that losses tend to zero together with $\gamma_3$, therefore this parameter plays a rather important role in the achievable transparency window bandwidth. If $\Omega_{ac}^2/4\gamma_1\gamma_3 \gg 1$, the right side of (13) becomes $\approx 4N_a|\mathcal{P}|^2\gamma_3/\Omega_{ac}^2$, so, at low values of $\gamma_3$, the decoherence term $\gamma_1$ contibutes very little to the absorption. The same can be done about the $\omega$-derivative of $\chi'$ at center frequency:

$$\left.\frac{d\chi'}{d\omega}\right|_{\omega_{ab}} \propto \frac{N_a|\mathcal{P}_{ab}|^2}{\gamma_1^2}\frac{1-\frac{\Omega_{ac}^2}{4\gamma_3^2}}{\left[1+\frac{\Omega_{ac}^2}{4\gamma_1\gamma_3}\right]^2} \tag{14}$$

For $\Omega_{ac}^2/4\gamma_3^2 \gg 1$ and $\Omega_{ac}^2/4\gamma_1\gamma_3 \gg 1$, the righ-hand side of (14) becomes $\approx 4N_a|\mathcal{P}_{ab}|^2/\Omega_{ac}^2$, independent of both coherence decay parameters. Clearly, both loss and refractive index will grow proportionally to both the atom number density and the dipole matrix element in the small-$\chi$ regime. Raising either one of these parameters will lead to higher dispersion and losses. The desired ratio between low-loss window and coupler bandwidth then has to be achieved through the control power; increasing the latter leads to smaller loss, however larger coupler bandwidth.

On the other hand, the same level of dispersion could

be obtained with shorter coherence times for higher $N_a$ or $|\mathcal{P}_{ab}|$; this is a highly desirable possibility given the very large dephasing rates observed in recent experiments in semiconductors [10]. Matrix elements can in principle be engineered in semiconductors through the proper design of coupled quantum wells [10], [11].

## IV. EIT directional coupler filter bandwidths

In the EIT directional coupler, the material of guide 1 is made to support EIT, while those of guide 2 and the substrate are regular semiconductor materials. Signal and control fields are input into guide 1. By an appropriate selection of the coupling length at the resonance frequency, only the signal beam is output from guide 2, assuming the control's frequency to be sufficiently phase-mismatched to stay in the launch waveguide. At null control power, the material in guide 1 displays a very large attenuation at center frequency, as shown in figure 3. On the other hand, a sufficiently intense control signal will cause the absorption to drop very strongly within a certain frequency range around the operation point. Within this low-loss window, the material dispersion will be extremely high, yielding, as explained above, a rather small bandwidth. In order to appreciate the enhanced selectivity of the EIT filter, the coupler designed in section II-B was considered. Refractive index and losses were obtained without approximation. The group index $n_{2g}$ is obtained from the angular-frequency version of (6) and replaced into 5 to yield the bandwidth. An analytical expression for the $\omega$-derivative of $n_{1p}$ can be obtained from (9). At center frequency, guide 1 has its original propagation constant, so the energy transfer is maximum. The coupler bandwidth as a function of the Rabi frequency $\Omega_{ac}$ is shown in Figure 4. As expected, very little

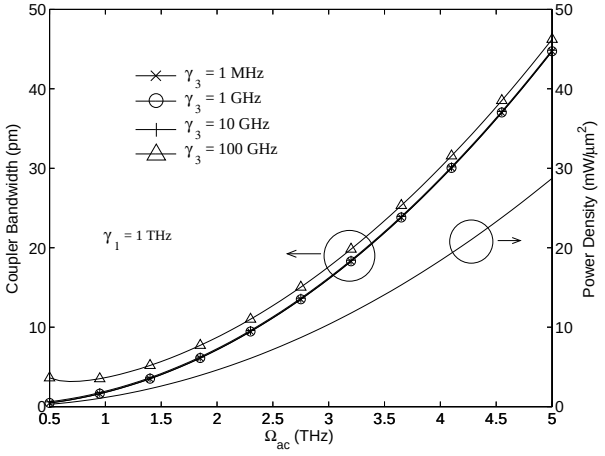


Fig. 4. EIT coupler bandwidth as function of $\Omega_{ac}$ for $\gamma_1 = 1$ THz and different values of $\gamma_3$.

change is observed in the coupler bandwidth for $\gamma_3$ varying between 1 MHz and 10 GHz, for the Rabi frequency range considered. Notice that the control signal power density as a function of $\Omega_{ac}$ is displayed in the figure as well, calculated from (8); it ranges approximately between 0.5 and 30 mW/$\mu m^2$. Sub-picometer bandwidths can be achieved at lower control signal powers. For $\gamma_3 = 100$ GHz , the bandwidth suffers a substantial increase at lower powers. At this point though, absorption at center frequency becomes rather high. We defined a transparency (or rather

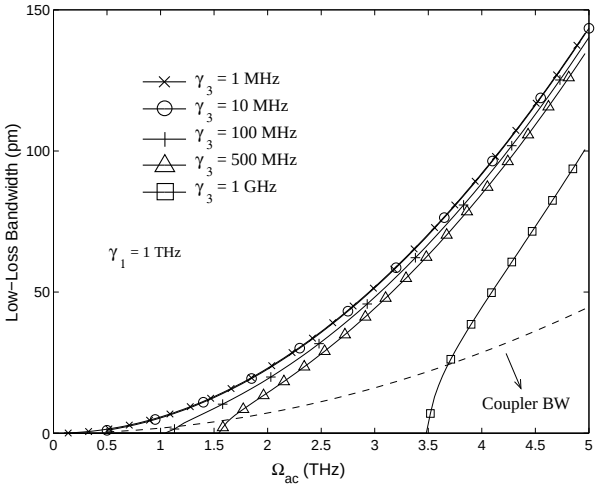


Fig. 5. Low-loss bandwidth as function of $\Omega_{ac}$ for $\gamma_1 = 1$ THz and different values of $\gamma_3$.

low-loss) window as the frequency range around the operation point where the overall losses for 1 $mm$ length of the EIT waveguide are less than 3 dB. It is expected that such transparency window can accomodate several narrow-bandwidth channels at the same time.

As shown in figure 5, the coherence decay constant $\gamma_3$ has a very strong impact on the loss bandwidth, since it controls the attenuation at center frequency. In fact, for larger values, losses at the operation frequency become higher than 3 dB for low control power, thus the low-loss window cannot be defined, e.g. for $\gamma_3$ at 1, 0.5 and 0.1 GHz, the low-loss window ceases to exist at $\Omega_{ac}$ below 3.5, 2.5 and 1.0 THz respectively. As compared to the coupler bandwidth for $\gamma_3 = 100$ MHz -which, as seen above, does not change much from that obtained with values two orders of magnitude higher or lower- it would be possible to accomodate up to three channels at the coupler bandwidth within the transparency window, for a control power density of about 30 $mW/\mu m^2$.

The loss bandwidth could in priciple be increased by decreasing the decoherence parameter between states $a$ and $b$, $\gamma_1$. This parameter influences the linewidth of the system's resonances, thus it has an obvious influence on the achievable low-loss window. Figure 6 shows the change in the low-loss bandwidth for different values of $\gamma_1$ and $\gamma_3 = 100$ MHz, within the same power density range. The coupler bandwidth is not significantly altered by this parameter as shown above, thus the same coupler bandwidth curve, shown as a dashed line in the picture can be used for comparison. For $\gamma_1 = 10$ GHz, A rather large low-loss bandwidth of 1.2 $nm$ can be achieved at 30 $mW/\mu m^2$ control power density, allowing for the accomodation of more than 20 40-picometer channels.

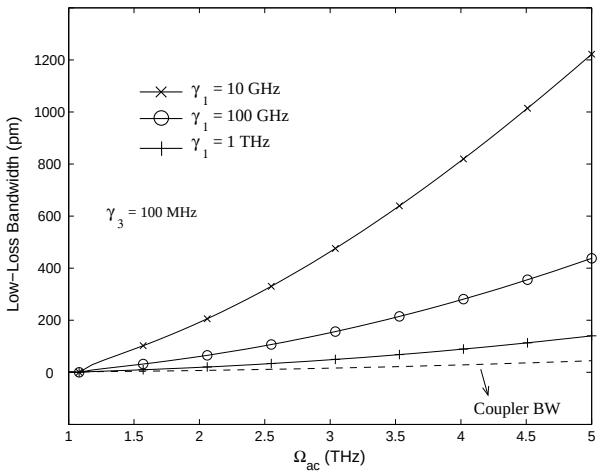


Fig. 6. Low-loss bandwidth as function of $\Omega_{ac}$ for $\gamma_3 = 100$ MHz and different values of $\gamma_1$.

## V. Implementation of EIT

The feasibility of the proposed device depends on the availability of a semiconductor system - or, in fact, any other material system - that allows EIT. With the development of molecular beam epitaxy (MBE) in the last decades, control of important parameters such as transition energies and matrix elements has become feasible in intersubband (IS) transitions [12] in high quality semiconductor quantum wells (QWs). IS transitions (ISTs) can be viewed as artificial atoms where the transition energies and dipole matrix elements can be engineered at will. IST-based schemes are thus interesting candidates for the implemetation of EIT in semiconductors. The first observation of EIT using ISTs was recently reported in InGaAs/InAlAs QWs [11]. Of special interest for EIT applications at 1.55 $\mu$m is the QW material InGaAs/AlAsSb [13]. This material can be grown lattice-matched on InP and the small effective electron mass ($m_e = 0.041$ at the band edge) and small LO-phonon energy ($\hbar\omega_{LO} = 32$ meV) in InGaAs entails lower scattering rates. Details of a possible implementation of a three-level system for EIT at $\lambda = 1.55$ $\mu$m, employing ISTs in coupled InGaAs/AlAsSb QWs, is shown Ref. [10].

The key issue to be addressed for the realization of EIT applications in semiconductor structures is the dephasing time ($T_2$). Experimentally determined dephasing times are still scarce, but $T_2 = 310$ fs (corresponding to $\gamma_1 = 0.5$ THz) was recently measured in 6 nm thick InGaAs/InAlAs QWs at $T = 8$ K [14]. In order to have low dephasing, important scattering mechanisms, i.e. electron-electron, electron-LO-phonon and interface roughness need to be controlled. For the dephasing of the b-c polarization the situation should be more favourable, since phase-space filling in these two lower states can considerably reduce the scattering rates. In an InGaAs/AlAsSb QW suited for IS absorption at $\lambda = 1.55\mu$m a dephasing time exceeding 1 ps, considering electron-electron and electron-LO-phonon processes, has been calculated for the ground state [15]. Thus a $T_2$ on the order 1 ps appears possible by improving material quality, either by an improved growth procedure or in a future QW material. At room temperature the situation is somewhat worse due to additional scattering processes. The longitudinal decay time ($T_1$) in semiconductors, i.e. here the IS relaxation time, is generally significantly longer than $T_2$ and should be of less concern.

There are a couple of solutions that may be used to significantly extend the coherence times; for example, it has been proposed to employ electron spin coherence, which can be orders of magnitude longer than for ISTs, to achieve EIT [16]. Another possibility to achieve lower dephasing than in an ordinary 2D electron gas is to use intraband transitions in quantum dots [17] rather than ISTs in QWs. Considering also non-semiconductor solutions, efficient EIT was quite recently demonstrated in rare-earth doped crystals [18].

## VI. Discussion and Conclusions

It is clear from section IV above that very narrowband, optically-controllable filtering characteristics can be achieved from an EIT coupler filter given that coherence times can be made sufficiently long. The values of $\gamma_1$ and $\gamma_3$ used here, though, are rather unrealistic when compared to what has been obtained experimentally so far in semiconductor systems.

A $\gamma_3$ on the order of 100 GHz corresponds to the 1 ps dephasing time mentioned above, three orders of magnitude larger than values used in the previous calculations. The same calculations show that, for $\gamma_3 = 100$ GHz and $\gamma_1 = 10 \times \gamma_3$, the narrowest achievable coupler bandwidth is close to 3.5 nm, with a loss bandwidth of the same order of magnitude, for $\Omega_{ac} \approx 40$ THz. This means that only one channel can be fit in the low-loss window. An improvement of $\gamma_3$ of one order of magnitude, on the other hand, yields a coupler bandwidth of 300 pm at $\Omega_{ac} \approx 13$ THz, with enough loss bandwidth to accommodate four channels. Additionally, some combinations of $\gamma_1$ and $\gamma_3$ will yield unrealistically large $\chi$ values. Although such $\gamma$ values are found in atomic systems, in general the atom number density, $N_a$, as well as the dipole matrix element $\mathcal{P}_{ab}$ are smaller than assumed here, leading to lower $\chi$.

In conclusion, we have shown the possibility of using the huge dispersion inherent in EIT to generate narrowband filters, with bandwidths several orders of magnitude smaller for a given length than what has hitherto been reported with more conventional mechanisms for generating differential dispersion.

**Acknowledgement**
Valuable discussions with Dr Björn Hessmo from the Royal Institute of Technology (KTH) are acknowledged.

## References

[1] K. Okamoto, "Fundamentals,technology and applications of AWGs", in *Proc. ECOC, 1998*, vol. 2, pp. 7-47.

[2] L. Thylén, "Wavelength and noise filtering characteristics of coupled active and passive waveguides",*IEEE J. Quantum Electron.*, vol. QE-23, pp. 1956-1961, Nov. 1987.

[3] P.-J. Rigole, S. Nilsson, E. Berglind, D.J. Blumenthal M. Shell, "State-of-the-art: Widely tunable lasers" in *Proc. SPIE (In-*

*Plane Semiconductor Lasers: from Ultraviolet to Midinfrared)* , 1997, vol. 3001, pp.382-393.

[4] M. O. Scully, M. S. Zubairy, *Quantum Optics*, Cambridge: Cambridge University Press, 1997, pp.225-230.

[5] L. Coldren, S. Corzine, *Diode Lasers and Photonic Integrated Circuits*, New York: John Wiley, 1995, pp. 281-296.

[6] J. Buus and M. J. Adams, "Phase and group indices for double heterostructure laser", *IEE Proc. Solid State Electron Devices*, vol. 3, pp. 189-195, Nov. 1979.

[7] H. Burkard, "Effective phase and group indices for $In_{1-x}Ga_xP_{1-y}As_y/InP$ waveguide structures", *J. App. Phys.*, vol. 55, pp. 503-508, Jan. 1984.

[8] M. Fleischhauer, M. D. Lukin, "Quantum memory for photons: Dark-state polaritons", *Phys. Rev. A* vol. 65, pp. 022314/1-12, Feb. 2002.

[9] K. Bergmann, H. Theuer, B. W. Shore, "Coherent population transfer among quantum states of atoms and molecules",*Rev. Mod. Phys.*, vol. 70, pp. 1003-1025, Jul. 1998.

[10] B. Hessmo, P. Holmström, L. Thylén, "Shaping Light Pulses Using Electromagetically Induced Transparency", presented at the Fifth International Symposium on Contemporary Technology, Tokyo, Japan, 2002.

[11] G.B. Serapiglia, E. Paspalakis, C. Sirtori, K.L.Vodopyanov, C.C. Phillips, "Laser-Induced Quantum Coherence in a Semiconductor Quantum Well", *Phys. Rev. Lett.*, vol. 84, pp. 1019-1022, Jan. 2000.

[12] L. C. West and S. J. Eglash,"First observation of an extremely large-dipole infrared transition within the conduction band of a GaAs quantum well", *Appl. Phys. Lett.*, vol. 46, p. 1156-1158, Jun. 1985.

[13] A. Neogi, T. Mozume, H. Yoshida and O. Wada,"Intersubband transitions at 1.3 and 1.55 $\mu$m in a novel coupled InGaAs/AlAsSb double-quantum-well structure", *Photon. Technol. Lett.*, vol. 11, pp. 632-634, Jun. 1999.

[14] R. A. Kaindl, S. Lutgen, M. Woerner, T. Elsaesser, B. Nottelman, V. M. Axt, T. Kuhn, A. Hase, and H. Künzel,"Ultrafast dephasing of coherent intersubband polarizations in a quasi-two-dimensional electron plasma",*Phys. Rev. Lett.*, vol. 80, pp. 3575-3578, Apr. 998.

[15] T. Akiyama, A. Neogi, H. Yoshida, and O. Wada,"Enhancement of optical nonlinearity for short wavelength ( 1.5 mu m) intersubband transitions by n-doped InGaAs/AlAsSb MQW", *Proc. CLEO*, 1999 p. 257.

[16] A. Imamoglu,"Electromagnetically induced transparency with twodimensional electron spins",*Opt. Commun.* vol. 179, pp. 179-182, May 2000.

[17] S. Sauvage, P. Boucaud, F. Glotin, R. Prazeres, J.-M. Ortega, A. Lemaî tre, J.-M. Gerard, and V. Thierry-Flieg,"Saturation of intraband absorption and electron relaxation time in n-doped InAs/GaAs self-assembled quantum dots",*Appl. Phys. Lett.*, vol. 73, pp. 3818-3820, Dec. 1998.

[18] B. S. Ham, P. R. Hemmer, M. S. Shariar,"Efficient electromagnetically induced transparency in a rare-earth doped crystal",*Optics Commun.*, vol. 144, p. 227-230, Dec. 2002.

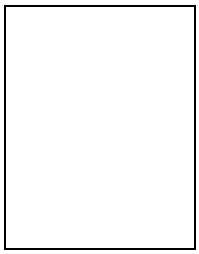

**Marcelo Davanço** obtained his B.S. and M.S. degrees in Electrical Engineering from the Universidade Estadual de Campinas (UNICAMP), Campinas, Brazil, in 1998 and 2000, respectively. He is now pursuing his Ph.D. degree also in Electrical Engineering at the University of California, Santa Barbara. He is mainly interested in the design, fabrication and application of integrated optical devices for optical communications.

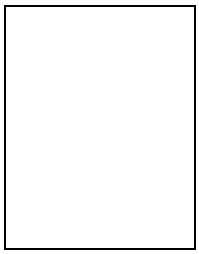

**Petter Holmström** was born in 1967 in Västerled, Sweden. He received the M.S. degree in engineering physics in 1996 from the Royal Institute of Technology (KTH), Stockholm, Sweden, where he is currently working toward the Ph.D. degree at the Laboratory of Optics, Photonics and Quantum Electronics. His research interests include intersubband transitions and their applications for optical communication.

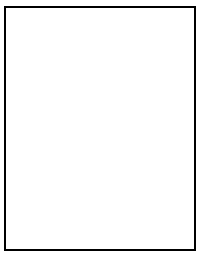

**Daniel J. Blumenthal** (M'97SM'02) received the B.S.E.E. degree from the University of Rochester, Rochester, New York, the M.S.E.E. degree from Columbia University, New York, and the Ph.D. degree from the University of Colorado at Boulder, in 1981, 1988, and 1993, respectively. In 1981, he was with StorageTek, Louisville, CO, in the area of optical data storage. In 1986, he was with Columbia University in the areas of photonic switching systems and ultra-fast all-optical networks and signal processing. From 1993 to 1997, hewas Assistant Professor in the School of Electrical and Computer Engineering, Georgia Institute of Technology, Atlanta. He is currently the Associate Director for the Center on Multidisciplinary Optical Switching Technology (MOST) and Professor in the Department of Electrical and Computer Engineering at the University of California, Santa Barbara. His current research areas are in optical communications, wavelength division multiplexing, photonic packet switched and all-optical networks, all-optical wavelength conversion, optical subcarrier multiplexing, integrated-optic chip scale WDM, and nanophotonic technologies. He has authored or co-authored over 100 papers in these and related areas. Dr. Blumenthal was recipient of a 1999 Presidential Early Career Award for Scientists and Engineers (PECASE) from the White House and the DoD, a 1994 National Science Foundations Young Investigator (NYI) Award, and a 1997 Office of Naval Research Young Investigator Program (YIP) Award. He has served as an Associate Editor for the IEEE PHOTONICS TECHNOLOGY LETTERS and the IEEE TRANSACTIONS ON COMMUNICATIONS. He was a Guest Editor for the IEEE JOURNAL OF LIGHTWAVE TECHNOLOGY Special Issue in Photonic Packet Switching Systems (December 1998). He served as the General Program Chair for the 2001 OSA Topical Meeting on Photonics in Switching and as Program Chair for the 1999 Meeting on Photonics in Switching. He has also served on numerous other technical program committees including the Conference on Optical Fiber Communications OFC (1997, 1998, 1999, and 2000) and the Conference on Lasers and Electrooptics CLEO (1999 and 2000). He is a Member of the Optical Society of America and the Lasers and Electrooptic Society.

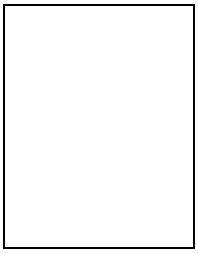

**Lars Thylén** (A'84–M'91) received the M.Sc. degree in electrical engineering and the Ph.D. degree in applied physics from the Royal Institute of Technology, Stockholm, Sweden, in 1972 and 1982, respectively. From 1973 to 1982, he was with SRA Communications, working in the areas of digital electronics, image processing, diffraction optics, and optical signal processing. From 1976 to 1982, he held a research position at the Institute of Optical Research, Stockholm, where he was engaged in research in integrated and guided wave optics, notably waveguide theory, RF spectrum analysis, and optical signal processing. In 1982, he joined Ericsson, heading a group doing research in the area of integrated photonics in lithium niobate and semiconductors and its applications to optical communications and switching. From 1985 to 1986, he was a Visiting Scientist with the Department of Electrical Engineering and Computer Sciences, University of California, Berkeley. He has also been a Visiting Scientist with the Optical Sciences Center, University of Arizona, Tucson. In 1987, he became an Adjoint Professor in the Department of Microwave Engineering, Royal Institute of Technology, Stockholm. He was active in the inception, planning, and running of the RACE I OSCAR project as well the RACE II MWTN (multiwavelength transport network) and ACTS METON projects, on which he has written a number of invited papers. Since 1992, he has been a Professor in the Department of Electronics, heading the Laboratory of Photonics and Microwave Engineering. From 1992 to 1997, he was a Consultant to Ericsson. Since 1996, he has been Program Director of the Swedish photonics research program, supported by the Swedish Foundation for Strategic Research. He is a Cofounder and Board Member of Optillion, Stockholm, a rapidly growing startup in the area of 10 Gb/s+ Ethernet transceivers. His current research interests include low-dimensional optics and electronics, devices for photonic switching, optical networks, and the physics involved in electronic and photonic switching operations. He has authored or coauthored more than 100 journal papers and conference contributions as well as a book chapter; served on program committees for major optics conferences. He has received 20 patents. Prof. Thylen is a member of the Optical Society of America (OSA) and served as Program Chair and General Chair for the 1995 and 1997 OSA Topical Meetings on Photonics in Switching, respectively.